KSCE Journal of Civil Engineering (2020) 24(2):561-568
DOI 10.1007/s12205-019-0978-1

pISSN 1226-7988, eISSN 1976-3808
www.springer.com/12205

Structural Engineering

2-D Reliable Crack Analysis by Enriched Petrov-Galerkin Natural Element Method

Jin-Rae Cho[a]

[a]*Member, Dept. of Naval Architecture and Ocean Engineering, Hongik University, Sejong 30016, Korea*

ARTICLE HISTORY

Received 31 May 2019
Revised 6 October 2019
Accepted 18 November 2019
Published Online 25 December 2019

KEYWORDS

Enriched PG-NEM
Near-tip stress distribution
Stress intensity factor (SIF)
Modified interaction integral
Quarter and half models

ABSTRACT

This paper introduces a 2-D enriched Petrov-Galerkin natural element method (enriched PG-NEM) for the reliable crack analysis. The total displacement is expressed as a linear combination of usual non-singular displacement field and the near-tip singular one. The former is approximated in terms of Laplace interpolation functions, and its strain and stress distributions are smoothened by the patch recovery technique. The unknown coefficients of the latter are determined by a coupled PG-NEM, and its strain and stress distributions are smoothened by the patch recovery technique. The validity of present method is justified through the evaluation of crack-tip stress distributions and the stress intensity factors (SIFs) through two numerical examples. It has been found that the proposed method effectively and successfully captures the near-tip stress singularity with the reasonable accuracy, even with the remarkably coarse grid, when compared with an extremely fine grid and the analytical and numerical reference solutions.

1. Introduction

All the natural phenomena exhibit the singular behavior in the vicinity of non-convex wedge where the wedge angle is greater than π (in radian). Here, the singular behavior is meant by a rapid increase of behavior in the radial direction towards the wedge tip. It was reported that this peculiar geometry-induced singularity occurs in order for the phenomenon has finite strain energy within a scope of continuum mechanics (Szabó and Babuška, 1991). A representative one is crack problem in fracture mechanics, where the wedge angle at the crack tip is 2π so that the crack-tip stress field exhibits the strongest $1/\sqrt{r}$ singularity (Broek, 1982). A common feature of this kind of singularity is that the singular behavior is restricted within a very small region near the wedge and its intensity abruptly increases as the evaluation point approaches the wedge tip. For this reason, the locally fine gradient meshes have been widely used for the finite element analysis to tackle the capturing of crack tip singularity (Zienkiewicz et al., 1989; Needleman and Tvergaard, 1994).

However, it is widely known that there is a limit to what one can obtain the level in capturing the near-tip stress with locally fine meshes. To overcome this limitation in the direct use of standard finite elements, a number of useful approaches were introduced (Fleming et al., 1997). The *J*–integral, the enrichment method (Benzley, 1976; Gifford and Hilton, 1978; Asareh et al., 2018) and the specially-devised singular crack tip elements would be representative. Here, the first approach is an indirect method in which the stress intensity factor (SIF) is firstly computed and then the near-tip displacement and stress fields are to be asymptotically expanded. Later, this method in line integration form has evolved to the *M*–interaction integral (Yau et al., 1980) in area integration form. Meanwhile, in the enrichment, finite elements are enhanced by including the crack-tip singular fields in either the trial functions or the basis functions. Singular crack tip elements are similar to the enrichment method in representing the near-tip singular fields, but those are implemented in the form of finite elements and arranged only around the crack tip (Tracey, 1971).

These methods/elements have been successfully employed and advanced for finite element analyses of engineering fracture mechanics problems during several decades. Furthermore, the crack analysis method and the enrichment method have been extending to meshfree methods since the late 1990s (Fleming et al., 1997; Ching and Batra, 2001; Rao and Rahman, 2003; Cho and Lee, 2014; Belinha et al., 2016; Labibzadeh et al., 2018; Scheel et al., 2019). Basically, the extension was motivated by

CORRESPONDENCE Jin-Rae Cho ✉ jrcho@hongik.ac.kr Dept. of Naval Architecture and Ocean Engineering, Hongik University, Sejong 30016, Korea

the high smoothness of interpolation functions used for meshfree methods. In particular, natural element method which is the last meshfree method is characterized by the highest smoothness of C^1–continuity (Sukumar and Moran, 1999; Cho, 2019). Moreover, differing from the conventional grid-point meshfree methods, it does not suffer from the difficulty in numerical enforcement of displacement boundary condition and Gauss integration. Particularly, Petrov-Galerkin natural element (PG-NEM) provides more accurate Gauss integration thanks to the consistency between Delaunay triangle and the integration region (Cho and Lee, 2006). Although meshfree methods provide the prominent features in the crack analysis, the reliability enhancement in capturing the near-tip stress singularity is still open.

In this connection, the purpose of current study is to propose an enriched PG-NEM and to explore whether and how much it increases the numerical accuracy in capturing the crack-tip singular stresses. The trial displacement function is expressed by a linear combination of Laplace interpolation functions and the near-tip asymptotic displacement field. According to the addition of assumed singular displacement field, the prescribed essential boundary condition is modified. The non-enriched stresses obtained using Laplace interpolation functions are smoothened by the patch recovery technique (Cho, 2016). Two numerical examples are taken to illustrate the proposed method, to investigate the NEM model and to examine the evaluation accuracy in capturing the near-tip stress singularity. It has been found, from the numerical experiments, that the proposed method effectively and successfully computes near-tip stress distributions and SIFs with the reasonable accuracy, particularly for the relatively coarse NEM grid, when compared with the very fine grid and the other reference solutions. Meanwhile, it has been found that the quarter model is better in aspect of the stress level but the stress distribution patterns are better at the half model.

2. 2-D Linear Elasticity of Cracked Body

As shown in Fig. 1, a cracked body $\Omega \in \Re^2$ with the boundary $\partial\Omega$ is characterized by a cornering angle of 2π and the upper and lower faces $\Gamma_c = \overline{\Gamma_c^+ \cup \Gamma_c^-}$. Owing to this geometric feature, the stress field exhibits the $1/\sqrt{r}$ singularity near the crack tip (Szabó and Babuška, 1991). Except for this geometry-induced singularity, the crack problem is expressed by usual boundary

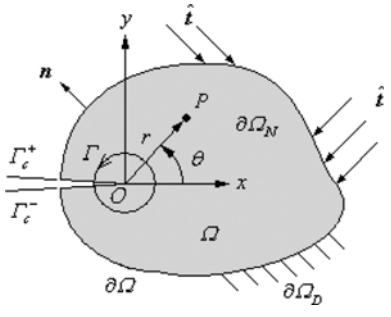

Fig. 1. A Cracked 2-D Linear Elastic Body

value problem (BVP) with the displacement and traction boundary regions $\partial\Omega_D$ and $\partial\Omega_N$. For the description of problem, a Cartesian co-ordinate system $\{O; x, y\}$ originated at the crack tip is used. Then, by denoting $\boldsymbol{u}(\boldsymbol{x})$ and $\boldsymbol{\sigma}$ be the displacement and Cauchy stress respectively, the BVP is governed by the equilibrium equations:

$$\nabla \cdot \boldsymbol{\sigma} = 0 \quad in \quad \Omega \tag{1}$$

together with the essential and natural boundary conditions given by respectively:

$$\boldsymbol{u} = \hat{\boldsymbol{u}} \quad on \quad \partial\Omega_D \tag{2}$$

$$\sigma \cdot \boldsymbol{n} = \begin{cases} \hat{\boldsymbol{t}} & on \quad \partial\Omega_N \\ 0 & on \quad \Gamma_c^{\pm} \end{cases} \tag{3}$$

In which $\boldsymbol{n}$ is an outward unit vector normal to $\partial\Omega$ and $\hat{\boldsymbol{t}}$ indicates the traction force.

In 2-D planar configuration, the stress intensity factor (SIF) which indicates the crack-tip stress singularity is usually evaluated by the J–integral given by:

$$J = \int_{\Gamma} \left(W\delta_{1j} - \sigma_{ij} \frac{\partial u_i}{\partial x_1'} \right) n_j ds \tag{4}$$

with $W = \boldsymbol{\sigma} \cdot \boldsymbol{\varepsilon} / 2$ being the strain energy density. The value J evaluated along an arbitrary closed path Γ around the crack tip is the energy release rate and independent of the integral path. This value is constituted with the SIFs as follows (Irwin, 1957): $J = \left(K_I^2 + K_{II}^2\right) / \overline{E}$, where $\overline{E}$ is E for plane stress while $E/(1-\nu^2)$ for plane strain. For non-mixed loading, the calculation of SIF is straightforward from the J–integral. But, for mixed loading, one should employ the interaction integral $M^{(1,2)}$ given by:

$$M^{(1,2)} = \int_{\Gamma} \left[W^{(1,2)}\delta_{1j} - \sigma_{ij}^{(1)} \frac{\partial u_i^{(2)}}{\partial x_1} - \sigma_{ij}^{(2)} \frac{\partial u_i^{(1)}}{\partial x_1} \right] n_j ds \tag{5}$$

for two equilibrium states 1 and 2. Here, the actual equilibrium state is chosen as state 1, while the asymptotic field for mode I or II is adopted for state 2. And, $W^{(1,2)} = \left[\boldsymbol{\sigma}^{(1)} \cdot \boldsymbol{\varepsilon}^{(2)} + \boldsymbol{\sigma}^{(2)} \cdot \boldsymbol{\varepsilon}^{(1)}\right] / 2$ indicates the mutual strain energy density for the combined state.

By expanding the contour Γ to a donut-type closed path $C = \Gamma + \Gamma_c^+ + \Gamma_o + \Gamma_c^-$ which is shown in Fig. 2 and introducing a specific smooth weighting function $q(\boldsymbol{x})$, one can transform the line integral (5) to the following area integral given by:

$$M^{(1,2)} = \int_A \left[\sigma_{ij}^{(1)} \frac{\partial u_i^{(2)}}{\partial x_1} + \sigma_{ij}^{(2)} \frac{\partial u_i^{(1)}}{\partial x_1} - W^{(1,2)}\delta_{1j} \right] \frac{\partial q}{\partial x_j} dA \tag{6}$$

The reader may refer to the references (Moës et al., 1999; Cho and Lee, 2014) for the detailed procedure of derivation. The weighting function q has unity along Γ, zero along Γ_o, and any value between 0 and 1 within the integral region A. The area integral (6) is more preferable than the line integral (5) because the line integration along path Γ becomes occasionally painstaking.

Returning to Eq. (4), the $J^{(1+2)}$ – integral for the combined

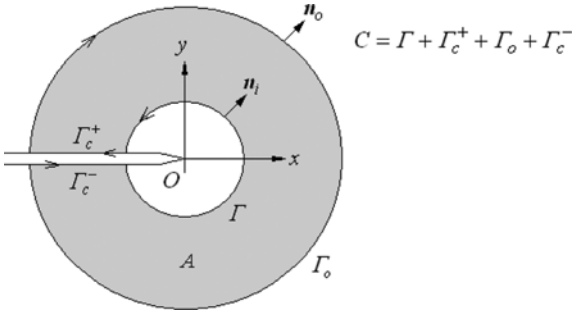

Fig. 2. An Extension of Closed Path C and an Integral Domain A

state is expressed by:

$$J^{(1+2)} = \int_{\Gamma}\left[\frac{1}{2}\left(\sigma_{ij}^{(1)}+\sigma_{ij}^{(2)}\right)\left(\varepsilon_{ij}^{(1)}+\varepsilon_{ij}^{(2)}\right)\delta_{1j} - \left(\sigma_{ij}^{(1)}+\sigma_{ij}^{(2)}\right)\frac{\partial\left(u_i^{(1)}+u_i^{(2)}\right)}{\partial x_1}\right] n_j ds$$
$$= J^{(1)} + J^{(2)} + M^{(1,2)} \tag{7}$$

Meanwhile, from the previous Irwin's relation $J = \left(K_I^2 + K_{II}^2\right)/\overline{E}$, it can be also represented as following:

$$J^{(1+2)} = \frac{1}{\overline{E}}\left[\left(K_I^{(1)}+K_I^{(2)}\right)^2 + \left(K_{II}^{(1)}+K_{II}^{(2)}\right)^2\right]$$
$$= J^{(1)} + J^{(2)} + \frac{2}{\overline{E}}\left(K_I^{(1)}K_I^{(2)} + K_{II}^{(1)}K_{II}^{(2)}\right) \tag{8}$$

Therefore, the M–integral is correlated with the stress intensity factors K_I and K_{II} such that:

$$M^{(1,2)} = \frac{2}{\overline{E}}\left(K_I^{(1)}K_I^{(2)} + K_{II}^{(1)}K_{II}^{(2)}\right) \tag{9}$$

Then, two stress intensity factors K_I and K_{II} could be evaluated by taking the closed form near-tip asymptotic displacement fields (Anderson, 1991) for state 2. The mode-I stress intensity factor K_I is evaluated according to:

$$K_I = \frac{\overline{E}}{2}M^{(1,\,\text{Mode I})} \tag{10}$$

by taking the mode-I near-tip asymptotic displacement for state 2, and vice versa for K_{II}.

3. Enriched Petrov-Galerkin Natural Element Method

The boundary value problem expressed by Eqs. (1) – (3) is converted to the weak form according to the principle of virtual work: Find $\boldsymbol{u}(\boldsymbol{x})$ such that:

$$\int_{\Omega}\varepsilon(\boldsymbol{v}) : \sigma(\boldsymbol{u})d\Omega = \int_{\partial\Omega_N}\hat{\boldsymbol{t}}\cdot\boldsymbol{v}\,ds \tag{11}$$

for every virtual displacement field $\boldsymbol{v}(\boldsymbol{x})$ in the Cartesian co-ordinate system $\{x, y\}$. In the Petrov-Galerkin natural element approximation for a non-convex natural element grid $\mathfrak{I}_{NEM}$ consisted of N nodes and a number of Delaunay triangles as represented in Fig. 3(a), trial and test displacement fields $\boldsymbol{u}(\boldsymbol{x})$ and $\boldsymbol{v}(\boldsymbol{x})$ are approximated as:

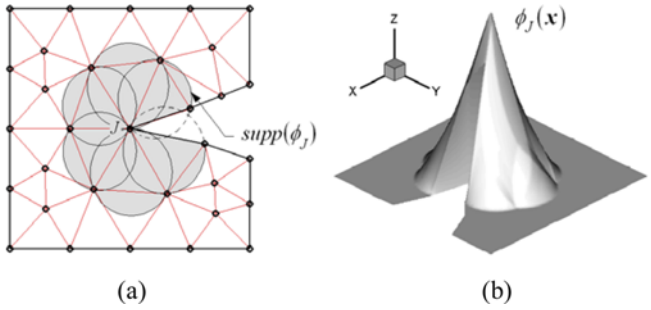

Fig. 3. Natural Element Method: (a) Non-convex NEM Grid $\mathfrak{I}_{NEM}$, (b) Laplace Interpolation Function $\phi_J(\boldsymbol{x})$ at the Crack Tip

$$\boldsymbol{u}_h(\boldsymbol{x}) = \sum_{J=1}^{N}\overline{\boldsymbol{u}}_J\phi_J(\boldsymbol{x}) + k_1\begin{bmatrix}Q_{11}(\boldsymbol{x})\\ Q_{12}(\boldsymbol{x})\end{bmatrix} + k_2\begin{bmatrix}Q_{21}(\boldsymbol{x})\\ Q_{22}(\boldsymbol{x})\end{bmatrix} \tag{12}$$

$$\boldsymbol{v}_h(\boldsymbol{x}) = \sum_{I=1}^{N}\overline{\boldsymbol{v}}_I\Psi_I(\boldsymbol{x}) + \lambda_1\begin{bmatrix}Q_{11}(\boldsymbol{x})\\ Q_{12}(\boldsymbol{x})\end{bmatrix} + \lambda_2\begin{bmatrix}Q_{21}(\boldsymbol{x})\\ Q_{22}(\boldsymbol{x})\end{bmatrix} \tag{13}$$

with Laplace interpolation functions $\phi_I(\boldsymbol{x})$ depicted in Fig. 3(b). Here, $\psi_I(\boldsymbol{x})$ are constant-strain finite element basis functions which are defined over Delaunay triangles.

Here, k_1 and k_2 are the crack-associated constants to be determined, and the functions $Q_{1\alpha}(\boldsymbol{x})$ and $Q_{2\alpha}(\boldsymbol{x})$ represent the near-tip displacement fields defined by:

$$Q_{11}(\boldsymbol{x}) = \frac{1}{2\mu}\sqrt{\frac{r}{2\pi}}\cos\left(\frac{\theta}{2}\right)\left[\kappa - 1 + 2\sin^2\left(\frac{\theta}{2}\right)\right] \tag{14}$$

$$Q_{12}(\boldsymbol{x}) = \frac{1}{2\mu}\sqrt{\frac{r}{2\pi}}\sin\left(\frac{\theta}{2}\right)\left[\kappa + 1 - 2\cos^2\left(\frac{\theta}{2}\right)\right] \tag{15}$$

$$Q_{21}(\boldsymbol{x}) = \frac{1}{2\mu}\sqrt{\frac{r}{2\pi}}\sin\left(\frac{\theta}{2}\right)\left[\kappa + 1 + 2\cos^2\left(\frac{\theta}{2}\right)\right] \tag{16}$$

$$Q_{22}(\boldsymbol{x}) = \frac{-1}{2\mu}\sqrt{\frac{r}{2\pi}}\cos\left(\frac{\theta}{2}\right)\left[\kappa - 1 - 2\sin^2\left(\frac{\theta}{2}\right)\right] \tag{17}$$

Referring to Fig. 1, r is the radial distance from the crack tip while θ is the angle from the x'–axis. Meanwhile, μ indicates the shear modulus and κ is the Kolosov constant given by:

$$\kappa = \begin{cases} 3-4\nu & \text{plane strain} \\ (3-\nu)/(1+\nu) & \text{plane stress}\end{cases} \tag{18}$$

with ν being the Poisson's ratio. From Eq. (23), the overall nodal coefficients $\overline{\boldsymbol{u}}_J$ are defined by:

$$\overline{\boldsymbol{u}}_J(\boldsymbol{x}) = \boldsymbol{u}_h(\boldsymbol{x}_J) - k_1\begin{bmatrix}Q_{11}(\boldsymbol{x}_J)\\ Q_{12}(\boldsymbol{x}_J)\end{bmatrix} - k_2\begin{bmatrix}Q_{21}(\boldsymbol{x}_J)\\ Q_{22}(\boldsymbol{x}_J)\end{bmatrix} \tag{19}$$

and the overall stress and strain fields corresponding to $\overline{\boldsymbol{u}}_J$ are recovered by the global recovery technique. Meanwhile, the original essential boundary condition (2) is modified as:

$$\hat{\boldsymbol{u}} = \hat{\boldsymbol{u}} - k_1\begin{bmatrix}Q_{11}(\hat{\boldsymbol{x}})\\ Q_{12}(\hat{\boldsymbol{x}})\end{bmatrix} - k_2\begin{bmatrix}Q_{21}(\hat{\boldsymbol{x}})\\ Q_{22}(\hat{\boldsymbol{x}})\end{bmatrix}, \quad \hat{\boldsymbol{x}} \quad on \quad \Gamma_D \tag{20}$$

Substituting Eqs. (12) and (13) into Eq. (22), together with

Eqs. (4) and (5), provides us:

$$\begin{bmatrix} \boldsymbol{K}_{IJ} & K_{I1} & K_{I2} \\ K_{I1}^T & K_{11} & K_{12} \\ K_{I2}^T & K_{12}^T & K_{22} \end{bmatrix} \begin{Bmatrix} \overline{\boldsymbol{u}}_J \\ k_1 \\ k_2 \end{Bmatrix} = \begin{Bmatrix} \boldsymbol{F}_I \\ f_1 \\ f_2 \end{Bmatrix} \tag{21}$$

In which the global stiffness matrices $\boldsymbol{K}_{IJ}$ and load vectors $\boldsymbol{F}_I$ are given by:

$$\boldsymbol{K}_{IJ} = \int_\Omega \boldsymbol{B}_I^T \boldsymbol{D} \boldsymbol{B}_J \, d\Omega, \quad \boldsymbol{F}_I = \int_{\Gamma_N} \Phi_I^T \hat{\boldsymbol{t}} \, ds, \qquad I, J = 1,2,\cdots,N \tag{22}$$

where,

$$\boldsymbol{B}_I^T = \begin{bmatrix} \phi_{I,x} & 0 & \phi_{I,y} \\ 0 & \phi_{I,y} & \phi_{I,x} \end{bmatrix} \tag{23}$$

$$\boldsymbol{D} = \frac{E}{(1+\nu)(1-2\nu)} \begin{bmatrix} 1-\nu & \nu & 0 \\ \nu & 1-\nu & 0 \\ 0 & 0 & \dfrac{1-2\nu}{2} \end{bmatrix} \quad \text{for plane strain} \tag{24}$$

Meanwhile, the enriched stiffness matrices $K_{\alpha\beta}$, load vectors f_α, and the interface matrices $K_{I\alpha}$ are defined by, respectively:

$$K_{\alpha\beta} = \int_\Omega \hat{\boldsymbol{B}}_\alpha^T \boldsymbol{D} \hat{\boldsymbol{B}}_\beta \, d\Omega, \quad f_\alpha = \int_{\Gamma_N} \hat{\phi}_\alpha^T \hat{\boldsymbol{t}} \, ds, \quad \alpha, \beta = 1,2 \tag{25}$$

$$K_{I\alpha} = \int_\Omega \boldsymbol{B}_I^T \boldsymbol{D} \hat{\boldsymbol{B}}_\alpha \, d\Omega \tag{26}$$

with

$$\hat{\phi}_\alpha^T = \left[Q_{\alpha 1}(\boldsymbol{x}), Q_{\alpha 2}(\boldsymbol{x}) \right] \tag{27}$$

$$\hat{\boldsymbol{B}}_\alpha = \begin{bmatrix} Q_{\alpha\alpha,x}(\boldsymbol{x}) \\ Q_{\alpha\beta,y}(\boldsymbol{x}) \\ Q_{\alpha\alpha,y}(\boldsymbol{x}) + Q_{\alpha\beta,y}(\boldsymbol{x}) \end{bmatrix}, \quad \alpha\alpha = \text{no sum} \tag{28}$$

Figure 4 schematically represents the identification of integral region A and the definition of weighting function $q(\boldsymbol{x})$ which are prerequisite for the numerical implementation of $\tilde{M}^{(1,2)}$ in Eq. (6). For these two things, first a circle of the radius r_{int} which is originated at the crack tip is imaginarily drawn on NEM grid. Then, the nodal values of $q(\boldsymbol{x})$ are assigned based on this circle such that unity is specified to all the interior nodes while zero to the outer remaining nodes. Then, referring to Fig. 2, the boundary of a square composed of eight darkened Delaunay triangles serves as an internal path Γ. On the other hand, the grayed region outside the internal path Γ automatically becomes an integral domain A. The configuration of outer boundary Γ_o influenced by the function type of $q(\boldsymbol{x})$, the present configuration is when Laplace interpolation function $\phi_I(\boldsymbol{x})$ is used to define $q(\boldsymbol{x})$. According to the properties of Laplace interpolation functions (Sukumar et al., 1998), the defined weighting function $q(\boldsymbol{x})$ becomes unity within a set of darkened Delaunay triangles while it has the values between zero and unity within the grayed integral domain A.

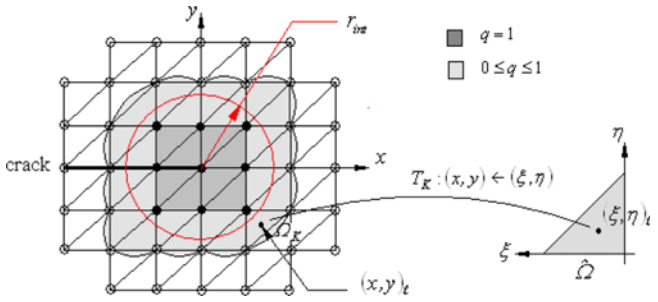

Fig. 4. A Crack Tip-Originated Circle and a Graded Integral Domain A

4. Numerical Experiment

The enriched NEM module was developed in Fortran and combined into the previously developed PG-NEM code (Cho and Lee, 2006) having the stress recovery module (Cho, 2016). To demonstrate and validate the present method, the crack problem of an infinite plate with collinear cracks depicted in Fig. 5(a) is considered. Differing from the cracks in plates of finite size which are of great practical interest, the present infinite plate with periodic cracks provides the closed form solution.

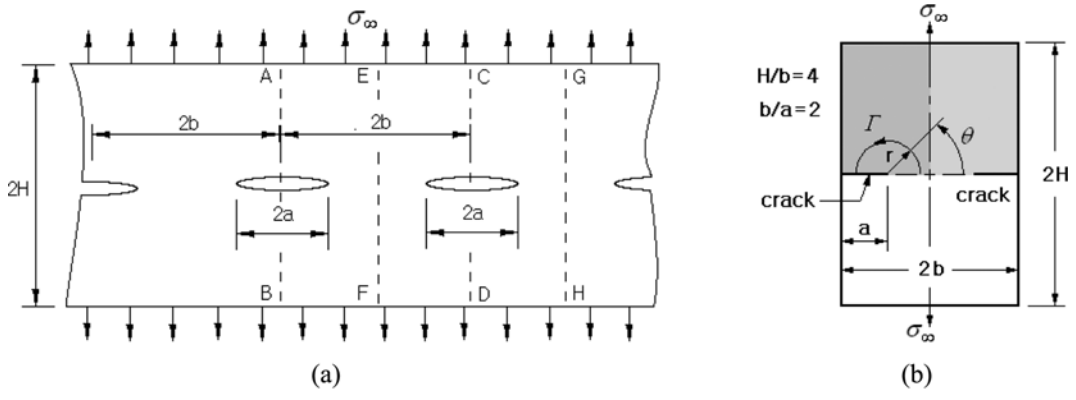

Fig. 5. An Infinite Plate with Collinear Cracks (Broek, 1982): (a) Geometry Dimensions and Loading, (b) Periodic Model with Double Edge Crackscks

Meanwhile, for the numerical study, one may take two kinds of periodic finite crack problems. One is obtained when the plate is cut along EF and GH, the other is if the plate is cut along AB and CD. Since the first one has been widely taken for the numerical studies, for examples (Ryicki and Kanninen, 1977; Chow and Atluri, 1995), the second periodic analysis model is taken for the current numerical experiments. Fig. 5(b) represents the detailed second periodic model, and the stress intensity factor for this double edge problem is calculated according to (Broek, 1982):

$$K_I = \sigma_\infty \sqrt{\pi a}\left(1.12\sqrt{\pi} + 0.76\left(\frac{a}{2b}\right) - 8.48\left(\frac{a}{2b}\right)^2 + 27.36\left(\frac{a}{2b}\right)^3\right) \tag{29}$$

with a being the half crack length. Where, a circular path Γ around the left crack tip has the relative radius $r/a = 0.0139$, and the near-tip stress distributions are to be evaluated along this circular path.

This double edge problem is in the plane strain state, and the Young's modulus E and Poisson's ration v are set by 200 GPa and 0.3. From the problem symmetry, two different symmetric models, quarter (1/4) and half models are simulated and compared using the present enriched PG-NEM. A darkened left upper quarter region is taken for the first 1/4 model, while a grayed entire upper region is chosen for the second 1/2 model. Fig. 6(a) show two uniform 11 × 41 and 21 × 41 NEM grids generated for 1/4 and 1/2 models, respectively, where the grayed region with the center of crack tip for evaluating SIFs is generated by specifying the value of r_{int}. This value was set by two times of the square of rectangular area of a pair of Delaunay triangles (Moës et al., 1999). Fig. 6(b) is a gradient fine NEM grid for 1/4 model which was generated for the comparison.

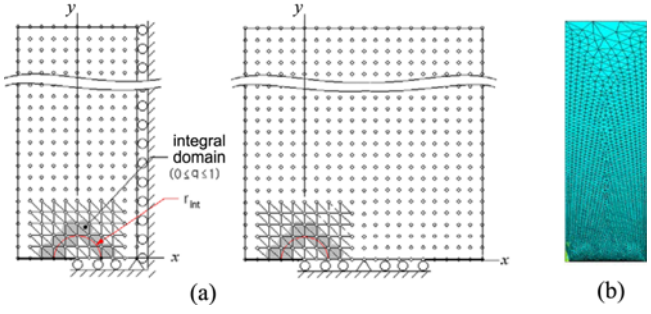

Fig. 6. NEM Models (grids): (a) Quarter (1/4) and Half Models, (b) A Gradient Fine NEM Grid (unit: m, N = 2,516)

The enrichment is applied to the NEM analyses using uniform NEM grids, but not to the NEM analysis using locally refined grid. Both the NEM analysis and the global stress recovery were carried out using 13 Gauss integration points. Figs. 7(a) – 7(c) comparatively represent the distributions of three normalized stress components σ_x/σ_∞, σ_y/σ_∞ and τ/σ_∞ along the circular path Γ shown in Fig. 5(b) with the relative radius of $r/a = 0.0139$. The theoretical values were referred to the reference (ASTM, 1965) in which the correction factor C is 1.02. Three cases provide the stress distributions similar to the exact ones, but the case without enrichment shows the remarkably low stress level. It implies that only the locally fine gradient grid without enrichment encounters the limitation in capturing the near-tip stress singularity. On the other hand, it is clearly observed that two uniform coarse grids (models) with enrichment provide the remarkably improved stress levels. Hence, it has been justified that the enrichment of interpolation function is effective to capture the near-tip singular stresses, even for coarse uniform NEM grids. Meanwhile, two enriched models show the difference in the stress level and the stress distribution. The difference between two models is not remarkable at σ_y, but it is not negligible at σ_x and τ. The 1/4 model is shown to be better in aspect of the stress level, but the stress distributions are better at the 1/2 model.

Next, the mode-I stress intensity factors (SIFs) were evaluated using the M–integral, and the evaluated values are compared with the analytic solutions (29) in Table 1. First of all, the case without enrichment provides the SIFs which are lower than the analytic ones. The maximum difference is found to be 13.18%.

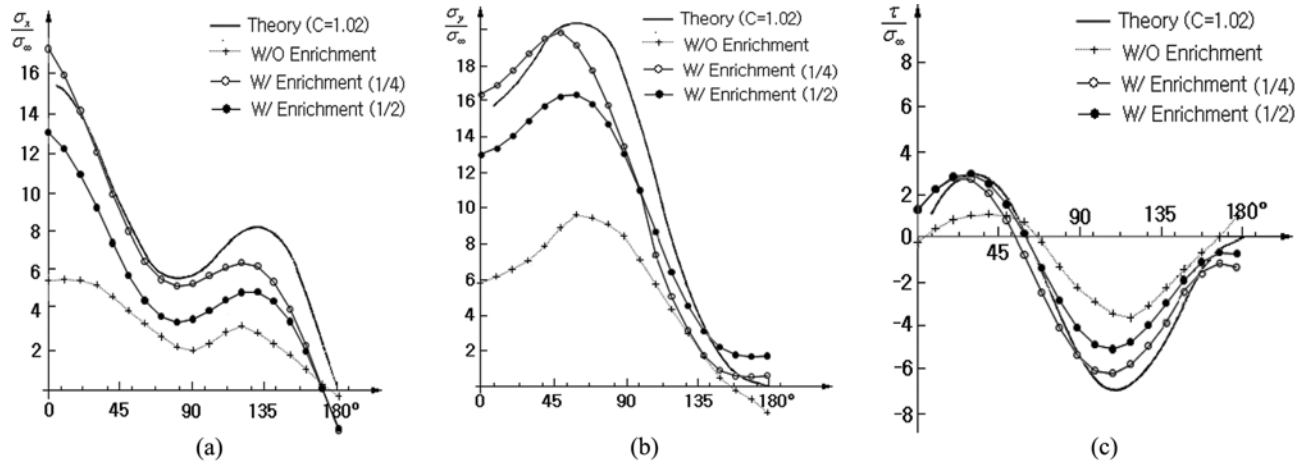

Fig. 7. Comparison of the Stress Distributions along the Circular Path (r/a = 0.0139): (a) σ_{xx}, (b) σ_{yy}, (c) τ

Table 1. Comparison of the Normalized Stress Intensity Factors $K_I / \sigma_\infty \sqrt{\pi a}$

Method	Crack length a						
	0.2	0.3	0.4	0.5	0.6	0.7	0.8
Broek (1982)	1.1332	1.1315	1.1406	1.1721	1.2375	1.3486	1.5167
Without enrichment	0.9838	0.9861	1.0023	1.0344	1.0909	1.1881	1.3677
With enrichment (1/4)	1.0499	1.1163	1.1607	1.2042	1.2611	1.3481	1.4857
With enrichment (1/2)	1.0505	1.1334	1.1747	1.2592	1.3032	1.3411	1.6292

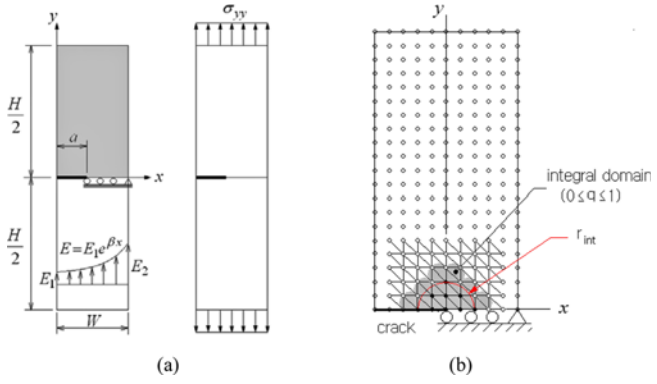

Fig. 8. An Inhomogeneous Rectangular Plate with an Edge Crack: (a) Geometry Dimensions and Boundary Conditions, (b) Uniform NEM Grid

Table 2. Normalized Stress Intensity Factors $K_I / \sigma_{yy} \sqrt{\pi a}$ for the FGM Plate with an Edge Crack

Method	Relative crack length a/W				
	E_2/E_1	0.2	0.3	0.4	0.5
Present method	0.1	1.3023	1.8429	2.5573	3.5041
	10	0.960	1.1501	1.5811	2.1757
Erdogan and Wu (1997)	0.1	1.2965	1.8581	2.5699	3.5701
	10	1.0019	1.2291	1.5884	2.1762
Kim and Paulino (2002)	0.1	1.2840	1.8460	2.5440	3.4960
	10	1.0030	1.2280	1.5880	2.1750
Rao and Rahman (2003)	0.1	1.3374	1.8976	2.5938	3.5472
	10	0.9958	1.2343	1.5980	2.1889

at $a = 0.2$. On the other hand, two enriched cases provide more accurate SIFs which are higher than the analytic ones. The maximum differences of two models are 7.35% for 1/4 model and 7.42% for 1/2 model. The 1/2 model leads to the SIFs which are slightly higher than those of the 1/4 model. But, the difference between two models is negligible such that the relative difference is less than 1.0%.

Next, we consider an inhomogeous plate shown in Fig. 8(a) with an edge crack under uniform tension, where $W = 1$ unit and $H/W = 8.0$ while a/W is variable as 0.2, 0.3, 0.4, 0.5 and 0.6 for the parametric study. The problem is in plane strain condition, and the Young's modulus varies in the form of $E(E) = E_1 \exp(\beta x)$ while Poisson's ratio is uniform as 0.3. The exponent index β is calculated according to $\beta = ln(E_2/E_1)$ with E_1 and E_2 being the elastic moluli at $x = 0$ and $x = L$, respectively. Here, E_1 is set by 1 unit and two cases of E_2/E_1 are chosen as follows: $E_2/E_1 = 0.1$ and 10.0, and the distribution loading is $\sigma_{yy}(x, \pm 4) = \pm 1.0$. The theoretical solution of this problem was provided by Erdogan and Wu (1997).

A darkened upper half is chosen for the NEM analysis from the problem symmetry, and the following symmetric boundary conditions are specified to the symmetric line. The vertical displacement constraint of $u_y = 0$ is specified to the symmetric line, and the lateral displacement constrain of $u_x = 0$ is prescribed to the right end of line. A 11 × 41 uniform NEM and 13 Gauss points were used for the NEM analysis, the stress recovery and the modified interaction integral $\tilde{M}^{(1,2)}$ (Rao and Rahman, 2003). Table 2 compares the normalized mode-I SIFs with other numerical results. It is observed that the SIFs evaluated by the proposed enriched PG-NEM are in good agreement with the analytical solution of Erdogan and Wu (1997) for all the combinations of E_2/E_1 and a/W with the maximum relative difference of 6.43%. In addition, it is clearly observed that the proposed method is correlated satisfactorily with Kim and Paulino (2002) and Rao and Rahman (2003), with the maximum relative difference of 7.32%.

5. Conclusions

In this paper, a 2-D enriched Petrov-Galerkin natural element method (enriched PG-NEM) was introduced for the reliable crack analysis. The trial function was enriched using the near-tip asymptotic displacement, and accordingly the essential boundary condition was modified. The non-singular global displacement was extracted and its stress field was smoothened by the stress recovery technique. An infinite plate with collinear cracks and an inhomogeneous plate with an edge crack were taken for the illustrative numerical experiments.

Through the numerical experiment of an infinite plate using a locally refined find grid without enrichment, quarter (1/4) and half full (1/2) coarse uniform grids (models) with enrichment, the following main observations are drawn:

1. The case without enrichment encounters the limitation in capturing the near-tip stress singularity, even with locally refined fine grid. In the evaluation of SIF, it provides the SIFs that are lower than the analytic ones, with the maximum relative difference of 13.18%.
2. On the other hand, the cases with enrichment successfully and remarkably enhance the level of near-tip singular

stresses. Also, in the evaluation of SIF, two enriched cases provide more accurate SIFs with the almost half of relative difference of the case without enrichment.

3. The comparison of two enriched cases, it was found that the 1/4 model is better in aspect of the stress level but, in aspect of stress distribution, the 1/2 model provides more similar distribution pattern to the theoretical one. In the evaluation of SIF, two enriched models provide almost the same results with the maximum relative difference smaller than 1.0%.

Meanwhile, through the numerical experiment of inhomogeneous plate with an edge crack under uniform tension, it has been observed that:

4. The proposed method provides SIFs that are in good agreement with both the analytical solution and the numerical results obtained by FEM and meshfree method with the maximum relative error of 7.32%.

Acknowledgements

This research was supported by Basic Science Research Program through the National Research Foundation of Korea (NRF) funded by the Ministry of Education (Grant No. NRF-2017R1D1A1B03028879). This work was supported by 2019 Hongik University Research Fund.

ORCID

Jin-Rae Cho http://orcid.org/0000-0002-5367-4012

References

Anderson TL (1991) Fracture mechanics: Fundamentals and applications, 1st edition. CRC Press, Boca Raton, FL, USA

Asareh I, Kim TY, Song JH (2018) A linear complete extended finite element method for dynamic fracture simulation with non-nodal enrichments. *Finite Elements in Analysis and Design* 152:27-45, DOI: 10.1016/j.finel.2018.09.002

ASTM (1965) Fracture toughness testing and its applications. American Society for Testing and Materials, West Conshohocken, PA, USA 381:43-51

Belinha J, Azevedo JMC, Dinis L, Natal Jorge, RM (2016) The natural neighbor radial point interpolation method extended to the crack growth simulation. *International Journal of Applied Mechanics* 8(1):1650006, DOI: 10.1142/S175882511650006X

Benzley SE (1976) Representation of singularities with isoparametric finite elements. *International Journal for Numerical Methods in Engineering* 10:1249-1259, DOI: 10.1002/nme.1620080310

Broek D (1982) Elementary engineering fracture mechanics. Martinus Nijhoff Publishers, London, UK

Ching HK, Batra RC (2001) Determination of crack tip fields in linear elastostatics by the meshless local Petrov-Galerkin (MLPG) method. *Computer Modeling in Engineering and Science* 2(2): 273-289

Cho JR (2016) Stress recovery techniques for natural element method in 2-D solid mechanics. *Journal of Mechanical Science and Technology* 30(11):5083-5091, DOI: 10.1007/s12206-016-1026-4

Cho JR (2019) Computation of mixed-mode stress intensity factors in functionally graded materials by natural element method. *Steel and Composite Structures* 31(1):43-51, DOI: 10.12989/scs.2019.31.1.043

Cho JR, Lee HW (2006) A Petrov-Galerkin natural element method securing the numerical integration accuracy. *Journal of Mechanical Science and Technology* 20(1):94-109, DOI: 10.1007/BF0291620

Cho JR, Lee HW (2014) Calculation of stress intensity factors in 2-D linear fracture mechanics by Petrov-Galerkin natural element method. *International Journal for Numerical Methods in Engineering* 98(11): 819-839, DOI: 10.1002/nme.4666

Chow WT, Atluri SN (1995) Finite element calculation of stress intensity factors for interfacial crack using virtual crack closure integral. *Computational Mechanics* 16(6):417-425, DOI: 10.1007/BF00370563

Erdogan F, Wu BT (1997) The surface crack problem for a plate with functionally graded properties. *ASME Journal of Applied Mechanics* 64:449-456, DOI: 10.1115/1.2788914

Fleming M, Chu YA, Moran B, Belytschko T (1997) Enriched element-free Galerkin methods for crack tip fields. *International Journal for Numerical Methods in Engineering* 40:1483-1504, DOI: 10.1002/(SICI)1097-0207(19970430)40:8<1483::AID-NME123>3.0.CO;2-6

Gifford LN, Hilton PD (1978) Stress intensity factors by enriched finite elements. *Engineering Fracture Mechanics* 10(3):485-496, DOI: 10.1016/0013-7944(78)90059-0

Irwin GR (1957) Analysis of stresses and strains near the end of a crack traveling a plate. *Journal of Applied Mechanics* 24:361-364

Kim JH, Paulino GH (2002) Finite element evaluation of mixed mode stress intensity factors in functionally graded materials. *International Journal for Numerical Methods in Engineering* 53:1903-1935, DOI: 10.1002/nme.364

Labibzadeh M, Tabatabaei SMJH, Ghafouri HR (2018) An efficient element free method for stress field assessment in 2D linear elastic cracked domains. *Computational and Applied Mathematics* 37(5): 6719-6737, DOI: 10.1007/s40314-018-0710-7

Moës N, Dolbow J, Belytschko T (1999) A finite element method for crack growth without remeshing. *International Journal for Numerical Methods in Engineering* 46:131-150, DOI: 10.1002/(SICI)1097-0207(19990910)46:1<131::AID-NME726>3.0.CO;2-J

Needleman A, Tvergaard V (1994) Mesh effects in the analysis of dynamic ductile crack growth. *Engineering Fracture Mechanics* 47(1):75-91, DOI: 10.1016/0013-7944(94)90239-9

Rao BN, Rahman S (2003) Mesh-free analysis of cracks in isotropic functionally graded materials. *Engineering Fracture Mechanics* 70:1-27, DOI: 10.1016/S0013-7944(02)00038-3

Ryicki EF, Kanninen MF (1977) A finite element calculation of stress intensity factors by a modified crack closure integral. *Engineering Fracture Mechanics* 9(4):931-938, DOI: 10.1016/0013-7944(77)90013-3

Scheel J, Ricoeur A, Krupka M (2019) Calculation of stress intensity factors with an analytical enrichment of the modified crack closure integral. *Procedia Structural Integrity* 18:268-273, DOI: 10.1016/j.prostr.2019.08.163

Sukumar N, Moran B (1999) C^1 natural neighbor interpolant for partial differential equations. *Numerical Methods in Partial Differential Equations* 15:417-447, DOI: 10.1002/(SICI)1098-2426(199907)15:4<417::AID-NUM2>3.0.CO;2-S

Sukumar N, Moran A, Belytschko T (1998) The natural element method in solid mechanics. *International Journal for Numerical Methods in Engineering* 43:839-887, DOI: 10.1002/(SICI)1097-0207(19981115)43:5<839::AID-NME423>3.0.CO;2-R

Szabó B, Babuška I (1991) Finite element analysis. John Wiley & Sons, New York, NY, USA

Tracey D (1971) Finite elements for determination of crack tip elastic stress intensity factors. *Engineering Fracture Mechanics* 3(3):255-265, DOI: 10.1016/0013-7944(71)90036-1

Yau JF, Wang SS, Cortern HT (1980) A mixed-mode crack analysis of isotropic solids using conservation laws of elasticity. *Journal of Applied Mechanics* 47:335-341, DOI: 10.1115/1.3153665

Zienkiewicz OC, Zhu JZ, Gong NG (1989) Effective and practical h-p-version adaptive analysis procedure for the finite element method. *International Journal for Numerical Methods in Engineering* 28(4):879-891, DOI: 10.1002/nme.1620280411